Disease-associated missense mutations in bestrophin-1 affect cellular trafficking and anion conductance

Vladimir M. Milenkovic[1], Elena Röhrl[2], Bernhard H. F. Weber[2,*] and Olaf Strauss[1,*]

[1]Experimental Ophthalmology, Eye Hospital, University Medical Center Regensburg, 93054 Regensburg, Germany
[2]Institute of Human Genetics, University of Regensburg, 93054 Regensburg, Germany
[*]Authors for correspondence (bweb@klinik.uni-regensburg.de; strauss@eye-regensburg.de)

Accepted 12 May 2011
Journal of Cell Science 124, 2988–2996

doi: 10.1242/jcs.085878

Summary

Bestrophin-1, an integral membrane protein encoded by the *BEST1* gene, is localized predominantly to the basolateral membrane of the retinal pigment epithelium. Mutations in the *BEST1* gene have been associated with Best vitelliforme macular dystrophy (BMD), a central retinopathy with autosomal dominant inheritance and variable penetrance. Over 120 disease-causing mutations are known, the majority of which result in amino acid substitutions within four mutational hot-spot regions in the highly conserved N-terminal half of the protein. Although initially thought to impair Cl^- channel function, the molecular pathology of BEST1 mutations is still controversial. We have analyzed the subcellular localization of 13 disease-associated BEST1 mutant proteins in polarized MDCK II cells, an established model of apical to basolateral protein sorting. Immunostaining demonstrated that nine of the 13 mutant proteins failed to integrate into the cell membrane. The defective proteins were predominantly retained in the cytoplasm, whereas wild-type bestrophin-1 revealed cell membrane localization. Functional analysis of I^- fluxes in HEK-293 cells showed that all mutants exhibited a significant reduction in anion conductance. Our data indicate that defective intracellular trafficking could be a common cause of BMD accompanied by impaired anion conductance, representing a loss of anion channel function that is probably due to mistargeting of mutant protein.

Key words: Best vitelliforme macular dystrophy, Bestrophin-1, Iodide flux, YFP-I152L, Missense mutation, Protein trafficking

Introduction

Mutations in the *BEST1* gene (MIM number 607854) have been shown to result in several types of retinal degeneration, such as Best vitelliforme macular dystrophy (BMD), autosomal dominant vitreoretinochoroidopathy (ADVIRC), adult-onset macular dystrophy (AVMD), autosomal recessive bestrophinopathy (ARB) and retinitis pigmentosa (Boon et al., 2009; Davidson et al., 2009; Xiao et al., 2010). Thus far, over 120 distinct mutations have been identified and associated with the respective disorder (see http://www-huge.uni-regensburg.de/BEST1_database/). Nearly all the disease-associated changes are missense mutations and predominantly affect the N-terminal half of the BEST1 protein, termed bestrophin-1 (Boon et al., 2009; Stohr et al., 2002).

Bestrophin-1 is strongly expressed in the retinal pigment epithelium (RPE), where it mainly localizes to the basolateral membrane (Gouras et al., 2009; Guziewicz et al., 2007; Marmorstein et al., 2000; Mullins et al., 2007; Mullins et al., 2005; Neussert et al., 2010). The RPE fulfills a multitude of functions that are essential for excitability and the structural integrity of the photoreceptors (Strauss, 2005). Mutations in bestrophin-1 therefore probably result in altered RPE function, subsequently contributing to disease. This sequence of events has been demonstrated by ocular coherence tomography in BMD patients (Pianta et al., 2003), post mortem eyes of BMD patients (Bakall et al., 2007; Mullins et al., 2007; Weingeist et al., 1982) and in canine (Guziewicz et al., 2007) and murine (Zhang et al., 2010) animal models, which reveal alterations of the RPE such as hypertrophy (Bakall et al., 2007; Guziewicz et al., 2007), lipofuscin accumulation (Bakall et al., 2007; Guziewicz et al., 2007; Mullins et al., 2005; Weingeist et al., 1982) and focal loss of RPE cells (Bakall et al., 2007; Guziewicz et al., 2007; Mullins et al., 2005). Patients affected with BMD characteristically have an absent or reduced light-peak in the electro-oculogram (Arden and Constable, 2006; Boon et al., 2009; Cross and Bard, 1974; Ponjavic et al., 1999; Renner et al., 2005; Wabbels et al., 2004; Weleber, 1989). Functionally, bestrophin-1 has been suggested to play a dual role as an anion channel (Fischmeister and Hartzell, 2005; Hartzell et al., 2005; Hartzell et al., 2008; Jentsch et al., 2002; Milenkovic et al., 2009; O'Driscoll et al., 2009; Qu et al., 2004; Sun et al., 2002) and also as a regulator of intracellular free Ca^{2+} homeostasis (Barro-Soria et al., 2010; Barro Soria et al., 2009; Burgess et al., 2008; Hartzell et al., 2008; Marmorstein et al., 2009; Neussert et al., 2010; Rosenthal et al., 2006; Yu et al., 2008; Zhang et al., 2010). Subsequent reports have suggested that bestrophin-1 also acts as HCO_3^- channel (Qu and Hartzell, 2008), and it might have a function as an ion channel in the membranes of cell organelles (Barro-Soria et al., 2010; Neussert et al., 2010).

Although a plethora of disease-associated mutations in BEST1 are known, little information about the molecular mechanisms by which these mutations affect bestrophin-1 function is available. For example, most mutations appear to disrupt Cl^- channel function, although experimental evidence purely relies on cellular overexpression of mutant protein, possibly reflecting spurious artifacts well known for this type of in vitro approach (Clapham, 1998; Jentsch et al., 2002). Topological analysis of mutant bestrophin-1 has suggested that a minor proportion of mutations located in the transmembrane domains (TMDs) of bestrophin-1

affect membrane topology by destabilizing TMD structure (Milenkovic et al., 2007). Finally, a recent study has demonstrated a mislocalized mutant bestrophin-1 associated with retinitis pigmentosa (Davidson et al., 2009).

Numerous missense mutations in genes encoding integral membrane proteins are associated with defective cellular trafficking (Aridor and Hannan, 2000; Cheng et al., 1990; Hume et al., 2009; Kausalya et al., 2006; Liu et al., 2001; Zhou et al., 1998). Most integral membrane proteins are co-translationally inserted into the membrane of the endoplasmic reticulum (ER), from where they subsequently traffic through the Golgi to the plasma membrane. This protein processing, however, appears to be rather inefficient, even for wild-type proteins. For instance, the cystic fibrosis transmembrane conductance regulator (CFTR) assembles with <50% efficiency. In the case of mutant CFTR protein, the efficiency of cellular membrane integration declines to <25% that of the wild-type protein (Kopito, 1999). Similar observations have been made for a number of other integral membrane proteins, such as epithelial sodium channel (ENaC), band 3 anion exchanger (SLC4A1) and nicotinic acetylcholine receptor (CHRNA) (Paulson et al., 1991; Rajan et al., 2001; Valentijn et al., 1998). Protein folding and stability studies have demonstrated that a single amino acid change is sufficient to reduce the folding efficiency in a protein from 50% at body temperature to below 10% (Guerois et al., 2002). Because the most common mechanism by which a single amino acid change leads to a disease phenotype is disturbance of protein trafficking or folding (Sanders and Myers, 2004), we examined the trafficking of BMD-related mutants in polarized cells. Use of such a cell system is particularly important for trafficking studies of bestrophin-1, given that this protein localizes to the basolateral membrane of the RPE, a highly polarized cellular monolayer (Marmorstein et al., 2000).

Here, we have analyzed 13 disease-associated missense mutations by studying the subcellular localization and anion conductance of the encoded proteins. Anion permeability was assessed by monitoring the fluorescence quench of YFP I152L by I^- ions, whereas the subcellular localization of mutant bestrophin-1 was determined in polarized MDCK II cells, a standard model to investigate cellular trafficking (Rodriguez-Boulan et al., 2005). Our findings show that the majority of the mutant proteins are retained in different intracellular compartments and are not targeted to the plasma membrane. All mutants have a reduced anion permeability, suggesting that defective intracellular trafficking is the most common molecular basis for the BMD phenotype.

Results

Expression and cellular localization of BMD-associated mutant bestrophin-1 proteins

To investigate whether BMD-associated missense mutations affect plasma membrane targeting, wild-type bestrophin-1 and 13 missense mutations, located in four mutational hot-spots of bestrophin-1 (White et al., 2000), were generated by site-directed mutagenesis and stably expressed in polarized MDCK II cells. The additional pore-affecting mutation S79C (Qu et al., 2004) was also examined (Fig. 1A). A mean transepithelial resistance (TER) of $194 \pm 46\ \Omega\ cm^2$, after correction for background resistance, verified the integrity of the MDCK II cell monolayers, which were subsequently used for immunostaining. All constructs were also

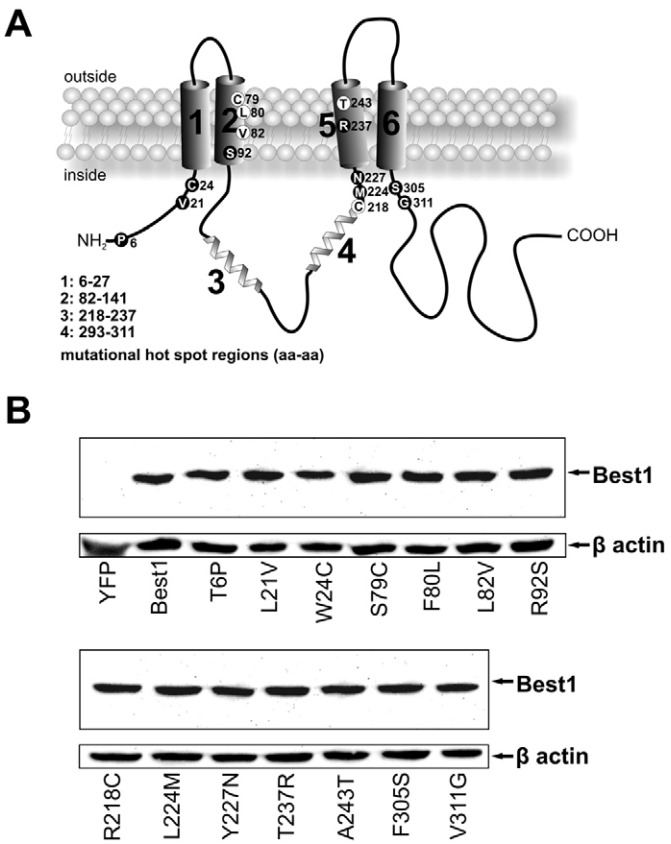

Fig. 1. Predicted topology of human bestrophin-1 and relative location of the disease-associated mutations analyzed in this study. (**A**) The mutated residues are numbered as in the human bestrophin-1 and are shown in single-letter code. The four mutational hot-spot regions identified by White et al. (White et al., 2000) are also indicated. The effect of the respective mutation, derived from colocalization studies (shown in Figs 2 and 3), on the predominant distribution of bestrophin-1 is indicated as either being in the plasma membrane (white background) or in intracellular compartments (black background). (**B**) Western blot analysis showing expression of the full-length bestrophin-1 constructs (67 kDa) in HEK-239 cells. β-Actin served as a loading control. The level of protein expression of the bestrophin-1 constructs were assessed by densitometry (supplementary material Fig. S1).

transiently expressed in HEK-293 cells. The wild-type and all mutant bestrophin constructs had comparable expression levels (Fig. 1B; supplementary material Fig. S1).

Polarized MDCK II cells expressing wild-type bestrophin-1 and the different bestrophin-1 mutants were co-stained for the integral membrane protein monocarboxylate transporter 1 (MCT-1). As expected, wild-type bestrophin-1 was targeted to the basolateral membrane and showed strong [Pearson's correlation coefficient (PCC) 0.92] colocalization with the plasma membrane marker MCT1 (Fig. 2A; Table 1). By contrast, nine out of the 13 bestrophin-1 mutants predominantly accumulated in the cytoplasm and revealed no colocalization with the MCT1 membrane protein (PCC 0.09–0.17) (Fig. 2B–J; Table 1). Several of the mutants (S79C, F80L, L82V and A243T) did show predominant localization to the plasma membrane (Fig. 3B–F; Table 1). However, compared with wild-type bestrophin-1, the efficiency of this localization was reduced. A Student's *t*-test analysis of the PCCs for the BMD-associated mutants and wild-type bestrophin-1 demonstrated a significant

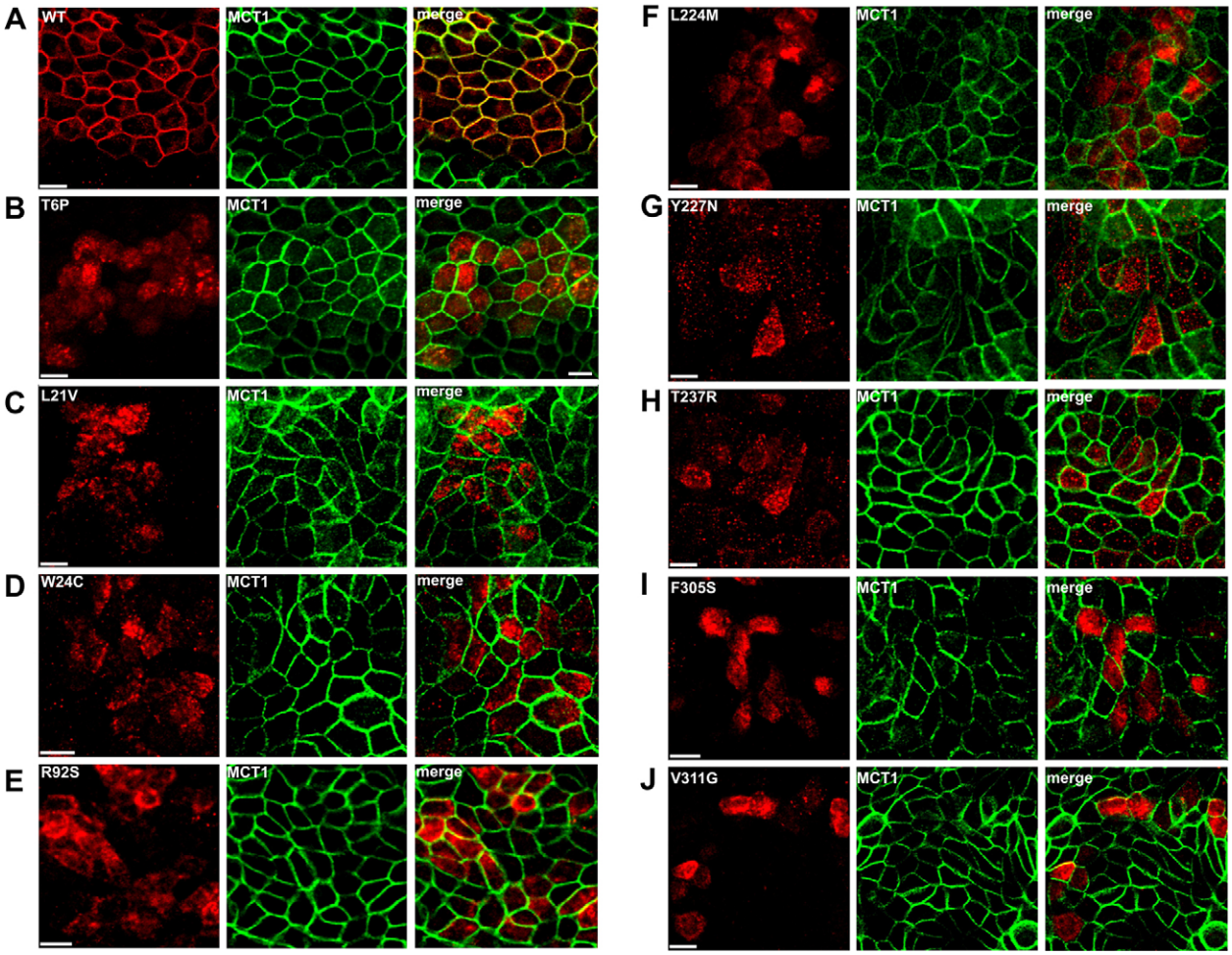

Fig. 2. Colocalization of bestrophin-1 mutants with the plasma membrane marker MCT-1 in MDCK II cells. (**A**–**J**) Monolayers of MDCK II cells stably expressing wild-type and various mutated bestrophin-1 constructs were stained with antibodies for human bestrophin-1 (left-hand panel, red) and MCT-1 (middle panel, green). Merged images (right-hand panel) show the extent of colocalization of bestrophin-1 mutants and MCT-1. As shown, bestrophin-1 mutants are predominantly targeted to the cytoplasm. The results of quantitative colocalization analysis are summarized in Table 1. Scale bars: 20 μm.

Table 1. Summary of steady-state localization of wild-type and mutant bestrophin-1 in MDCK II cells

			Colocalization with			
Bestrophin-1 form	Surface expression	Average PCC with MCT1	ER	Golgi	EEA1	LAMP1
Wild-type	+	**0.92**				
T6P	–	0.13				
L21V	–	0.17	+	*+	+	–
W24C	–	0.11				
S79C	+	**0.71**				
F80L	+	**0.75**				
L82V	+	**0.61**				
R92S	–	0.14	–	*+	–	–
R218C	+	**0.88**				
L224M	–	0.11	+	*+	+	–
Y227N	–	0.11				
T237R	–	0.15				
A243T	+	**0.56**				
F305S	–	0.09	–	–	*+	–
V311G	–	0.12				

Quantitative colocalization with the plasma membrane marker MCT1 was used to differentiate between surface and intracellular expression of bestrophin-1 ($n \geq 9$). Values in bold indicate significant colocalization with MCT1; +, colocalization; –, no colocalization; *, predominant steady-state localization.

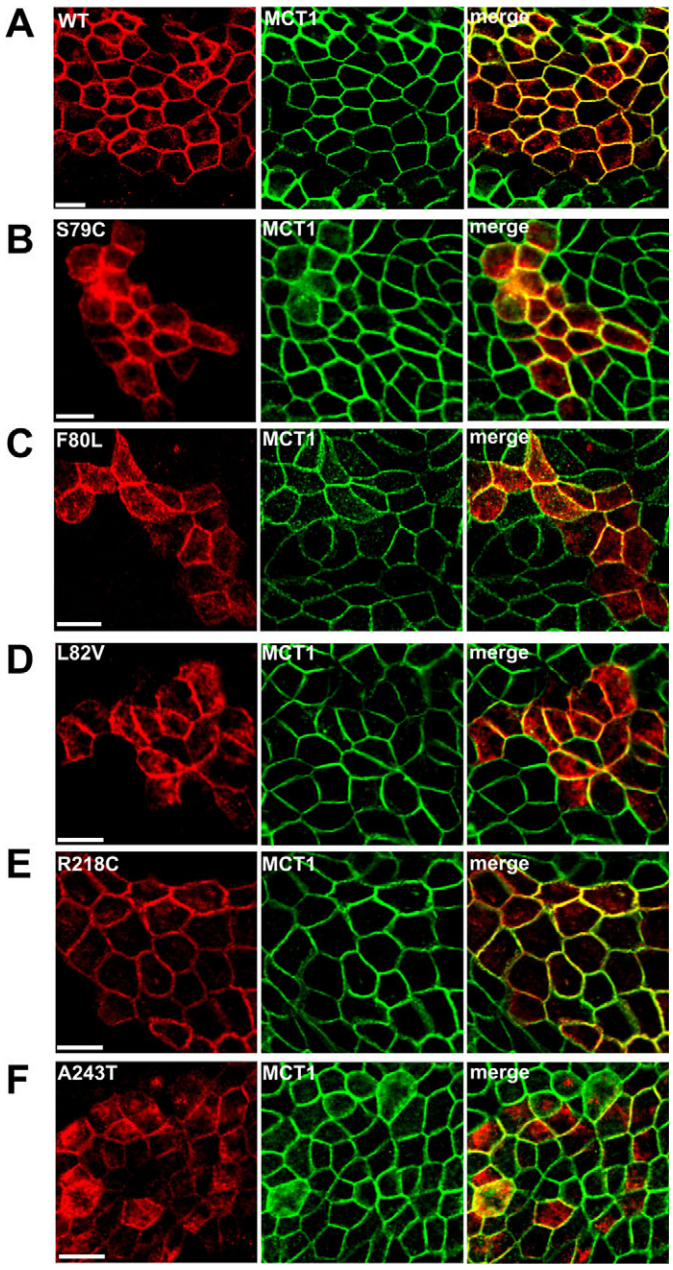

Fig. 3. Colocalization of bestrophin-1 mutants with the plasma membrane marker MCT-1 in MDCK II cells. (**A**–**F**) Monolayers of MDCK II cells stably expressing wild-type and various mutated bestrophin-1 constructs were stained with antibodies for human bestrophin-1 (left-hand panel, red) and MCT-1 (middle panel, green). Merged images (right-hand panel) show the extent of colocalization of bestrophin-1 mutants and MCT-1. As shown, bestrophin-1 mutants are predominantly targeted to the plasma membrane. The results of quantitative colocalization analysis are summarized in Table 1. Scale bars: 20 μm.

difference ($P<0.0001$) between the subcellular localization of all the mutants examined with the exception of mutant protein R218C, which had an intracellular distribution highly similar to wild-type bestrophin-1 ($P>0.05$) (Fig. 3E; Table 1).

Some of the mutants were studied in more detail by confocal imaging to obtain vertical optical sections across MDCK II cell monolayers. MDCK II monolayers were properly polarized as demonstrated by co-staining with the tight-junction protein zonula occludens-1 (ZO-1) and MCT-1 (Fig. 4A). In the polarized monolayers, wild-type bestrophin-1 colocalized with MCT1 to the basolateral part of the cell (Fig. 4B). By contrast, the F305S mutant protein, which is mistargeted to the cytoplasm (Fig. 2I), showed diffuse intracellular staining throughout the cell (Fig. 4C). However, the R218C mutant protein, which seems not to affect plasma membrane targeting (Fig. 3E), R218C almost completely colocalized to the basolateral membranes with MCT1 (Fig. 4D).

Bestrophin-1 mutants with defective membrane targeting localize to the Golgi complex, the ER or to early endosomes

Next, we aimed to identify intracellular compartments to which bestrophin-1 mutants with predominant intracellular distribution could localize. In order to clearly conclude about a possible mechanism we concentrated on mutant bestrophin-1 with predominant cytosolic localization. MDCK II cells stably expressing the bestrophin-1 mutants L21V, R92S, L224M or F305S, each one representing a mutational hot-spot of BEST1, were co-stained with anti-bestrophin-1 antibody and antibodies against the early endosome marker EEA1 (Fig. 5A), the Golgi complex marker GM130 (Fig. 5B), the ER marker BIP (Fig. 5C) and the lysosomal marker LAMP1 (Fig. 5D). All four mutants showed no noticeable overlap with the lysosomal marker. By contrast, mutants L21V, R92S and L224M extensively colocalized with the Golgi marker. Mutants L21V, L224M and F305S also colocalized with ER and early endosome markers. Mutant F305S had the least colocalization with all the subcellular markers tested. In order to more clearly identify the subcellular compartments in which mutant bestrophin-1 proteins are trapped, colocalization experiments were performed in subconfluent MDCK II cells (supplementary material Fig. S2). These results suggest that bestrophin-1 mutants mainly accumulate in the Golgi complex and the ER.

BMD-associated mutant bestrophin-1 proteins show decreased anion permeability of the cell membrane

To investigate the impact of missense mutations on the ability of bestrophin-1 to increase anion permeability of the cell membrane, I^- fluxes were measured by halide-sensitive YFP I152L fluorescence quench. As MDCK II cells are known to endogenously express a large variety of ion channels including Ca^{2+}-dependent Cl^- channels, these cells are largely unsuitable for use in expression systems to study ion channel function (Lang and Paulmichl, 1995; Rothstein and Mack, 1990; Shen et al., 2002). Accordingly, HEK-293 cells were triple-transfected with different bestrophin-1 constructs, YFP I152L and human P2Y purinoceptor 2 receptor (P2Y2). In a first step, extracellular Cl^- ions were replaced by I^-, which led to no quenching of the YFP I152L fluorescence (Fig. 6A). To stimulate Ca^{2+}-dependent anion conductance of the cell membrane, cells were exposed to 100 μM ATP. In cells co-transfected with YFP I152L and P2Y2, activation of endogenous anion channels contributed to a modest decrease in the YFP I152L fluorescence. By contrast, cells additionally transfected with wild-type bestrophin-1 showed a strong quench in YFP I152L fluorescence when ATP was applied indicating an influx of I^- ions into the fluorescence. Thus, the presence of bestrophin-1 increased the membrane permeability for anions. The mutant bestrophin-1 constructs T6P, L21V,

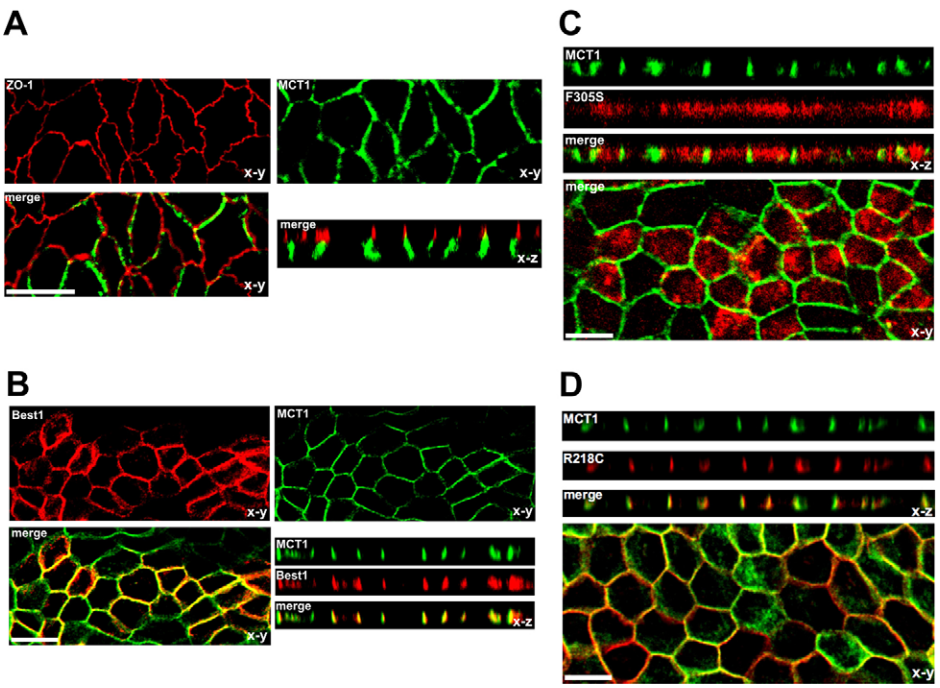

Fig. 4. *Z*-stack image analysis of representative bestrophin-1 mutants in MDCK II cells. (**A**) *Z*-stack image analysis of endogenous MCT-1 and ZO-1 in polarized MDCK II cells grown on the filter. ZO-1 shows apical localization, whereas MCT-1 localizes to the basolateral membrane. (**B**) Wild-type bestrophin-1 colocalizes with MCT-1 and is targeted to the basolateral membrane. (**C**) The F305S mutant is predominantly retained in the cytoplasm. (**D**) The R218C mutant is targeted to the plasma membrane, as shown from the colocalization with MCT-1 (Table 1). Shown are *x–y* and *x–z* projections of monolayers of MDCK II cells. Scale bars: 20 μm.

L82V, Y227N and F305S showed a strongly reduced ability to increase the anion permeability of transfected HEK-293 cells (Fig. 6A,B) despite a expression level comparable to the wild-type protein (Fig. 1B; supplementary material Fig. S1). By contrast, expression of the other nine mutant bestrophin-1 constructs (W24C, S79C, F80L, R92S, R218C, L224M, T237R, A243T and V311G) led to an anion permeability that was significantly higher than that of cells transfected with YFP I152L alone ($P<0.05$) (Fig. 6B).

Discussion

To gain further insight into the molecular mechanisms leading to BMD pathology, we examined intracellular trafficking of mutant bestrophin-1 proteins in polarized MDCK II cells. We analyzed 13 known disease-associated mutations and one mutation (S79C) that has been predicted to change the properties of the anion channel pore (Qu et al., 2004). Eight of these mutations (L21V, W24C, F80L, L82V, L224M, T237R, F305S and V311G) were functionally investigated for the first time, whereas none of the known BMD mutations had been examined in polarized epithelial cells previously. As a general theme, we found that the mutants analyzed either failed to traffic to the cell membrane or showed reduced efficiency to incorporate into the cell membrane, with exception of mutation R218C, which was targeted to the plasma membrane in a manner similar to the wild-type protein. Interestingly, colocalization of wild-type bestrophin-1 and MCT-1, a typical marker for the basolateral membrane, was not entirely congruent, as a small proportion of bestrophin-1 appeared to be associated with the lateral membrane, but it also localized within the cytoplasm. Similar observations have been made previously in other studies and were thought to implicate bestrophin-1 in Ca^{2+} signaling by the ER (Barro-Soria et al., 2010; Neussert et al., 2010). In a human airway epithelial cell line endogenously expressing bestrophin-1, wild-type bestrophin-1 had been previously found to be localized in the endoplasmic reticulum by co-staining of bestrophin-1 and calreticulin, calnexin or Stim-1 (stromal interacting molecule-1) (Barro-Soria et al., 2010). Furthermore, by co-staining of bestrophin-1 and β-catenin or pan-cadherin in native porcine RPE, we identified a proportion of bestrophin-1 close to the basolateral membrane but not integrated into the membrane (Neussert et al., 2010).

A refined colocalization analysis with various subcellular markers revealed that the mutants L21V, R92S, L224M and F305S were partially retained in the Golgi complex, the endoplasmic reticulum and in the early endosomes. This suggests that mutant bestrophin-1 proteins are synthesized in the ER and move to the Golgi complex where they fail to undergo further processing. Proteins with missense mutations located on regions of bestrophin-1 that reside in the cytoplasm (T6P, L21V, W24C, L224M, Y227N, T237R, F305S and V311G) showed a tendency to a more severe trafficking defect than mutations located in the transmembranal areas of bestrophin-1 (S79C, F80L, L82V and A243T). Thus, regions that localize to cytoplasm seem to be important for proper processing. Trafficking impairment might have been expected from mutations T6P, L21V and W24C as they are located in the N-terminus before the first transmembrane domain of bestrophin-1. Often, the immediate N-terminal structures guide proteins into vesicles, making trafficking to the cell membrane possible (Denzer et al., 2000; von Heijne, 1996). The mutants Y227N, T237R and V311G also showed disturbed trafficking, although the precise mechanism remains elusive. We speculate that these bestrophin-1 mutants also fail to process properly. In association with single BEST1 mutations, a marked phenotypic variability has been observed within families that show inheritance of single BEST1 mutations (Boon et al., 2009). Thus we cannot draw conclusions from the severity of trafficking defects to a possible phenotype.

To further investigate the properties of the disease-associated bestrophin-1 mutations, anion conductance was measured by halide-sensitive YFP I152L assays in transfected HEK-293 cells.

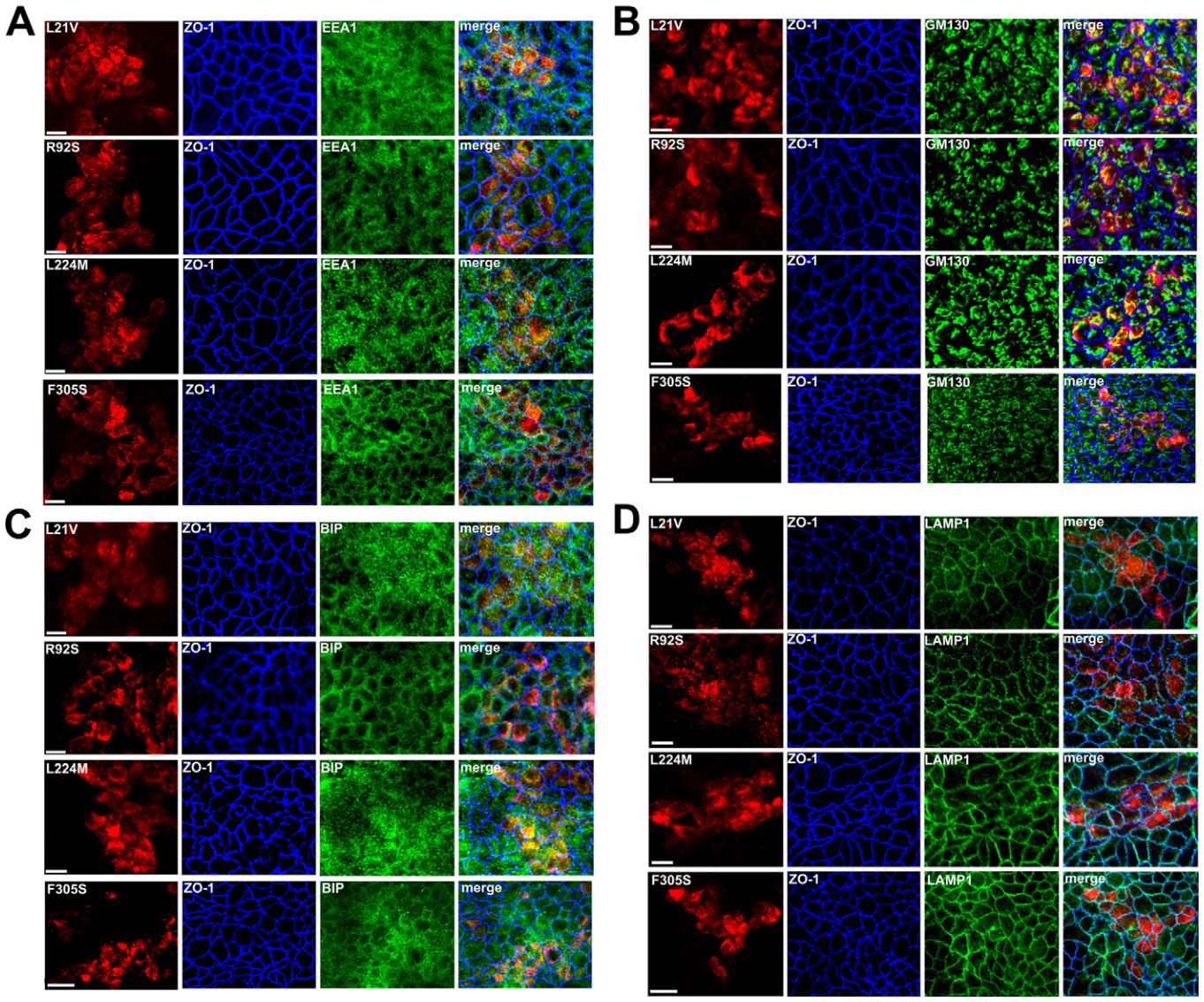

Fig. 5. Subcellular localization of representative bestrophin-1 mutants. Bestrophin-1 constructs, with missense mutations selected from each mutational hot-spot, were stably expressed in MDCK II cells and immunostained for bestrophin-1 (red), ZO-1 (blue) and the early endosome marker EEA1 (**A**), the Golgi marker GM130 (**B**), the ER marker BIP (**C**) or the lysosomal marker LAMP1 (**D**) (green). Merged images show the extent of colocalization. The mutants L21V, R92S and L224M extensively colocalized with GM130. The mutants L21V, L224M and F305S also colocalized with BIP and EEA1. F305S was least colocalized with all the subcellular markers. Scale bars: 20 μm.

HEK-293 cells are an established model for studying heterologously expressed ion channels (Varghese et al., 2006), and most data on bestrophin-1 ion channel function have been obtained with measurements in this cell line (Hartzell et al., 2008; Pusch, 2004). To increase cytosolic free Ca^{2+}, the cells were additionally transfected with the human P2Y2 receptor and stimulated with ATP. This is more physiological than the alternative approach using Ca^{2+} ionophores because stimulation of P2Y2 receptors involves activation of a physiological signal transduction cascade including generation of either Ins(1,4,5)P_3. Analysis of activation mechanisms of Ca^{2+}-dependent Cl^- channels in the RPE showed marked differences between the application of either Ins(1,4,5)P_3 or a Ca^{2+} ionophore (Strauss et al., 1996). As a main observation we found that all mutant bestrophin-1 led to a strongly reduced increase in Ca^{2+}-dependent anion permeability; the observed I^- quenches were significantly smaller than those seen with wild-type bestrophin-1. This observation is in accordance with patch-clamp data with the same or similar mutations in bestrophin-1 (Qu et al., 2009; Sun et al., 2002; Yu et al., 2006). Interestingly, nine of the mutant bestrophin-1 proteins (W24C, S79C, F80L, R92S, R218C, L224M, T237R, A243T and V311G) had significantly increased Ca^{2+}-dependent anion permeability compared with those from cells transfected with YFP I152L plus hP2Y2 alone. Thus, although activity was still much lower than with normal bestrophin-1, these mutations still have residual ion-conductance function.

Mutants S79C, F80L and R92S showed strongly reduced ability to increase Ca^{2+}-dependent anion permeability compared with wild-type bestrophin-1, and mutant L82V failed to increase

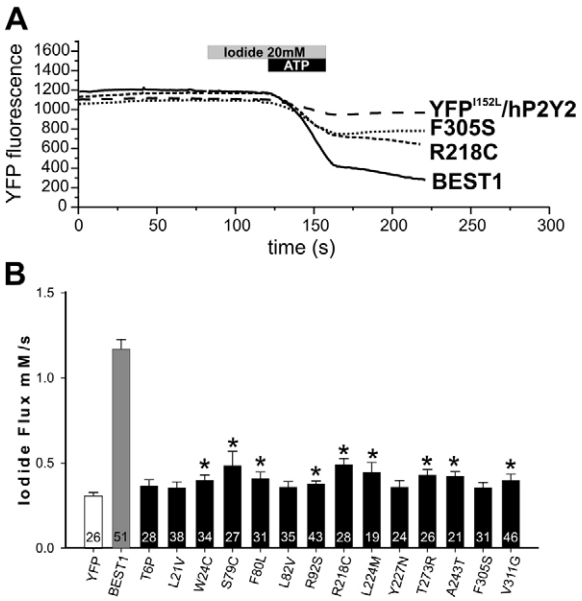

Fig. 6. Anion permeability of HEK-293 cells expressing mutant and wild-type bestrophin-1. (**A**) Purinergic activation of wild-type and selected mutated bestrophin-1 constructs in HEK-293 cells. Activation of Ca^{2+} activated Cl^- channels was measured by I^- influx measurements using the I^-sensitive protein YFP I152L (YFP^{I52L}). The figure shows examples of single measurements from cells which either express YFP I152L with human P2Y2 (hP2Y2) alone or YFP I152L with P2Y2 together with either wild-type bestrophin-1 or the mutant forms. (**B**) A summary of the effects of ATP stimulation on I^- uptake in HEK-293 cells expressing various bestrophin-1 constructs. All mutant bestrophin-1 showed significantly decreased I^- permeability compared with that of cells expressing wild-type bestrophin-1. However, the mutants W24C, S79C, F80L, R92S, R218C, L224M, T237R, A243T and V311G showed a significantly larger I^- permeability compared with cells which express YFP I152L with P2Y2 alone. The number of cells is given in the bar. $*P<0.05$.

the anion permeability. These mutations are located in the putative pore region that localizes around amino acid positions 70–90. Interestingly, S79C, a mutant not known to be associated with BMD, was utilized previously to demonstrate a putative pore region in the homologue bestrophin-2 (Qu et al., 2004; Xiao et al., 2010) but failed to increase the Ca^{2+}-dependent anion conductance in our experimental setup. The loss of I^- permeability of the mutant S79C is probably has a different cause to that of pathogenic mutants with comparable trafficking behavior because the mutation affects the putative pore. Therefore, the loss of I^- permeability might be explained by strongly changed ion selectivity and a subsequent decrease in I^- conductance of the pore. Despite its ability to localize to the plasma membrane, the R218C mutation failed to increase Ca^{2+}-dependent anion permeability in transfected HEK-293 cells. Thus, it is probable that the main effect of this mutation is a loss of anion channel function rather than a trafficking defect.

It should be mentioned that I^- flux experiments do not permit us to directly draw conclusions about ion channel properties of bestrophin-1 and its mutant forms. As it discussed previously by several groups, bestrophin-1 might have a function in the cytosol to regulate intracellular Ca^{2+} signaling, with changes in the anion conductance or permeability secondary to these effects (Barro-Soria et al., 2010; Barro Soria et al., 2009; Kunzelmann et al., 2009; Neussert et al., 2010; Zhang et al., 2010). This was mainly concluded from experiments where cells were transfected with bestrophin-1 together with the Ca^{2+}-dependent Cl^- channel anoctamine-1 (Ano1). In these cases, bestrophin-1 changed the membrane conductance for Cl^- by modulation of Ca^{2+} signaling and not by providing a membrane conductance for Cl^- by itself (Barro-Soria et al., 2010). Thus, our observations on I^- flux changes by bestrophin-1 and its mutant forms could also reflect altered Ca^{2+} signaling in response to P2Y2 receptor stimulation. Because the spatial distribution of Ca^{2+} signals is of importance for their regulative effects (Berridge et al., 2000; Petersen et al., 2001), it might well be that an altered subcellular distribution of bestrophin-1 leads to altered spatial distribution of Ca^{2+} signals and a subsequently altered activation of anion conductance.

Our data provide new insight into the molecular disease pathology of bestrophin-1 mutations. It appears that mutations located in the N-terminal region of bestrophin-1 result in a loss of function by impaired trafficking to the cell membrane, by a loss of pore function or by a combination of both. A loss of function in the disease-associated mutant proteins could explain the observed reduction of the light-peak in the electro-oculogram of BMD patients (Hartzell et al., 2008; Marmorstein et al., 2009; Xiao et al., 2010). The decreased anion conductance in the RPE probably influences transepithelial transport of Cl^- ions and water and might also impair volume regulation. Both properties are essential to RPE function and might cause disturbances in the interaction of photoreceptor outer segments and the RPE (Strauss, 2005).

Materials and Methods

Cell culture

HEK-293 (ATCC, cat# CRL-1573) and MDCK II (ATCC, cat# CCL-34) cells were cultured in Dulbecco's modified Eagle's medium (DMEM) containing L-glutamine, 4500 mg/l glucose and 110 mg/l sodium pyruvate. All media were supplemented with 10% (v/v) fetal calf serum and 1% (v/v) penicillin-streptomycin (PAA, Cölbe, Germany). Cells were cultured at 37℃, under an atmosphere with a relative humidity of 95% and containing 5% CO_2. HEK-293 cells were transfected with Lipofectamine 2000 transfection reagent (Invitrogen) following the manufacturer's instructions. MDCK II cells were transfected by electroporation using ECM 830 (BTX Harvard Apparatus, Holliston, MA, USA). Cells stably expressing wild-type and mutant bestrophin-1 were cultured for 2 weeks in a selection medium containing 500 µg/ml G418 (PAA). Pools of at least three independent stable colonies were used for immunofluorescent studies.

Transepithelial electrical resistance

Transepithelial electrical resistance of the MDCK epithelial monolayers was monitored with the Endohm apparatus (World Precision Instruments, Sarasota, USA). MDCK II monolayers were grown on Transwell polycarbonate filters (0.4 µm pore size), which consist of tissue-culture-treated polyester membranes with an insert diameter of 12 mm and an effective growth area of 1 cm^2. The upper chamber (apical side) contained 0.5 ml medium and the lower one (basolateral side) contained 1.8 ml medium. MDCK cells were seeded at a density of 10^5 cells per ml and were grown to reach a stable TER, representing a confluent monolayer, generally 5 days after seeding. The medium was changed every 2 days. The TER was normalized to the area of the filter after removal of the background resistance of a blank filter submerged in medium only. TER was measured in ohms cm^2 (Ω cm^2). The average TER measurement of polycarbonate filters in the absence of a cell monolayer was 120 Ω cm^2 (baseline).

Site-directed mutagenesis of BEST1

Full-length *BEST1* was amplified by reverse transcriptase (RT)-PCR from mRNA from human RPE and was directionally cloned into the pCDNA3 vector. Missense mutations were generated on a full-length *BEST1* cDNA template (GenBank accession number, NM_004183; 1764 bp in length encoding 585 amino acids), applying the QuikChange site-directed mutagenesis kit (Stratagene). The constructs were made with the primer pair combinations given in supplementary material Table S1. The final BEST1 constructs were fully sequenced to ensure the targeted mutagenesis had occurred correctly and to exclude the presence of

undesired sequence alterations. Sequencing reactions were performed with the Big Dye terminator cycle sequencing kit version 3 or 3.1 (Applied Biosystems) according to the manufacturer's instructions and were analyzed in an ABI Prism Model 3100 or 3730 sequencer (Applied Biosystems).

Cellular YFP I152L fluorescence measurement

HEK-293 cells were triple transfected using equal amount of each plasmid (encoding YFP I152L, P2Y2–His_6 receptor and the bestrophin-1 mutants). At 12–16 hours after transfection, cells were seeded onto 18-mm diameter round glass cover slips, and subsequent measurements were performed 36 hours after transfection. The YFP I152L plasmid was kindly provided by Luis J.V. Galietta, (Istituto Giannina Gaslini, Genova, Italy) (Galietta et al., 2001), and plasmid encoding human P2Y2–His_6 (Milenkovic et al., 2009) receptor was kindly provided by Karl Kunzelmann (Institut für Physiologie, Regensburg, Germany). Double immunostaining of the bestrophin-1 and P2Y2 receptor in HEK-293 cells, which were used for the I^- flux measurements, showed that majority of transfected cells expressed both proteins (data not shown). YFP fluorescence was excited at 500 nm with a polychromatic illumination system for microscopic fluorescence measurements VisiChrome (Visitron, Puchheim, Germany), and light emission was measured at 535 ± 15 nm with a photomultiplier detector (SF, Zeiss, Göttingen, Germany). Quenching of YFP I152L fluorescence by I^- influx was induced by replacing 20 mM extracellular Cl^- by I^- ions (Galietta et al., 2001). Images were acquired with a Coolsnap HQ CCD camera (Visitron, Puchheim, Germany) and processed with the Metafluor software (Visitron). HEK-293 cells were grown on 18-mm diameter round glass cover slips and mounted in an imaging chamber maintained at room temperature. Cells were continuously perfused at 4–5 ml per min with Ringer's solution. Cells were exposed to 20 mM I^- by replacing NaCl with equimolar NaI and maintaining the total concentration of NaCl plus NaI at 137 mM. Typically, measurements of fluorescence intensity were performed in groups of 5–15 transfected HEK-293 cells and represent the average intensity of all fluorescent cells within the selected area. Initial fluorescence values were similar among cells transfected with different *BEST1* cDNA constructs. The decrease of cell fluorescence caused by addition of NaI was analyzed to calculate anion transport. The fluorescence decay phase was fitted with an exponential function to derive the maximal slope. Maximal slopes were converted into rates of variation of intracellular anion concentration (in mM/s) using the equation: $d[X^-]/dt = K_X[d(F/F0)/dt]$, where $[X^-]$ is the anion concentration, K_X is the affinity constant of YFP for a I^- anion (Galietta et al., 2001) and F/F0 is the ratio of the cell fluorescence at a given time compared with the initial fluorescence.

Quantitative colocalization analysis

To analyze colocalization quantitatively, MDCK II cells stably expressing wild-type or mutant bestrophin-1 proteins were grown on filters and double labeled with anti-bestrophin-1 and anti-MCT-1 antibodies. After subsequent incubation with secondary antibodies conjugated with Alexa Fluor 488 and 543 (Invitrogen), filters were mounted in confocal matrix (Micro Tech Lab, Graz, Austria), and then examined with a confocal microscope LSM 510 (Zeiss, Göttingen, Germany). All images were taken as single sections in the *z*-plane. Double fluorescence for green and red channels was recorded after excitation of an argon-krypton-neon laser at wavelengths of 488 nm and 543 nm, respectively. Double-stained images were obtained by sequential scanning for each channel to eliminate the crosstalk of chromophores and to ensure reliable quantification of colocalization. Emission of the different fluorophores was detected using the appropriate filter sets and multi-channel acquisition. Quantitative analysis was performed with the software package ImageJ (Abramoff et al., 2004). Pearson's correlation coefficient (PCC) was employed to evaluate colocalization according to Abramoff (Abramoff et al., 2004). PCC is one of the standard techniques applied in pattern recognition for matching one image to another in order to describe the correlation of the intensity distributions between channels. It only takes into consideration the similarity of shapes between two images, and does not depend upon image pixel intensity values. Values of PCC range from –1 to 1, where –1 indicates no overlap and 1 is a complete colocalization.

Immunohistochemistry

For the immunofluorescence experiments, MDCK II cells stably expressing wild-type and mutant bestrophin-1 were grown on permeable supports (Costar Transwells, Fischer Scientific, Schwerte, Germany). Cells were fixed for 10 minutes at room temperature with 4% (w/v) paraformaldehyde. After three washing steps with 1× PBS, cells were permeabilized with blocking-permeabilization solution [10% (v/v) normal goat serum, 0.5% (v/v) Triton X-100 in 1× PBS] for 30 minutes. Cells were then labeled overnight with antibodies against bestrophin-1 (ab2182, mouse monoclonal) (Marmorstein et al., 2000), MCT-1, (ab35944, rabbit polyclonal), GM-130 (ab52649, rabbit polyclonal) (Shaheen et al., 2009), GRP78 BIP (ab21685, rabbit polyclonal) (Dykstra et.al., 2010) (all Abcam, Cambridge, UK), LAMP1 and EEA1 (both mouse monoclonal antibodies, BD Biosciences, Heidelberg, Germany) diluted 1:100–1:500 in 2% normal goat serum and 0.1% Triton X-100 in 1× PBS. Antibodies against ZO-1 (rat monoclonal, R26.4C, Developmental Studies Hybridoma Bank, University of Iowa, USA) specifically stain tight junctions. After three additional washing steps, cells were incubated for 1 hour with appropriate secondary antibodies (conjugated with Alexa Fluor 488, Alexa Fluor 546 and Alexa Fluor 633; Invitrogen). Cells were mounted in confocal matrix (Micro Tech Lab, Graz, Austria) and examined with a confocal microscope LSM510 (Carl Zeiss, Göttingen, Germany).

Western blotting

Protein lysates from transiently transfected HEK-293 cells were analyzed by SDS-PAGE and western blotting (Milenkovic et al., 2009) with antibodies against bestrophin-1 diluted 1:5000 (ab2182, Abcam, Cambridge, UK) and β-actin diluted 1:20,000 (Sigma). Quantification of protein expression was achieved by densitometry analysis of western blots with the help of a digital imaging analysis system (Chemiimager, Biozym, Oldendorf, Germany).

Data presentation and statistical analysis

All experiments were performed independently at least three times. Statistical significance was tested with the unpaired Student's *t*-tests, with $P<0.05$ considered significant.

We thank Elfriede Eckert and Andrea Dannullis for expert technical assistance, Karl Kunzelmann for providing the human P2Y2–His_6 expression vector and the rabbit polyclonal antibody against human bestrophin-1, Eugen Kerkhoff for helping with high-resolution microscopy to analyze colocalization with organelles, Miriam Breunig, Pharmazeutische Technologie, Regensburg for providing access to confocal microscopy, Enrique Rodriguez-Boulan for fruitful discussions and helpful suggestions and Myriam Mirza for editing the manuscript. This work was supported in part by grants from the Deutsche Forschungsgemeinschaft (STR480/9-2 and STR480/10-1, WE1259/16-2 and WE1259/20-1).

Supplementary material available online at
http://jcs.biologists.org/lookup/suppl/doi:10.1242/jcs.085878/-/DC1

References

Abramoff, M. D., Magelhaes, P. J. and Ram, S. J. (2004). Image processing with imageJ. *Biophotonucs Int.* **11**, 36-43.

Arden, G. B. and Constable, P. A. (2006). The electro-oculogram. *Prog. Retin. Eye Res.* **25**, 207-248.

Aridor, M. and Hannan, L. A. (2000). Traffic jam: a compendium of human diseases that affect intracellular transport processes. *Traffic* **1**, 836-851.

Bakall, B., Radu, R. A., Stanton, J. B., Burke, J. M., McKay, B. S., Wadelius, C., Mullins, R. F., Stone, E. M., Travis, G. H. and Marmorstein, A. D. (2007). Enhanced accumulation of A2E in individuals homozygous or heterozygous for mutations in BEST1 (VMD2). *Exp. Eye Res.* **85**, 34-43.

Barro Soria, R., Spitzner, M., Schreiber, R. and Kunzelmann, K. (2009). Bestrophin-1 enables Ca2+-activated Cl- conductance in epithelia. *J. Biol. Chem.* **284**, 29405-29412.

Barro-Soria, R., Aldehni, F., Almaca, J., Witzgall, R., Schreiber, R. and Kunzelmann, K. (2010). ER-localized bestrophin 1 activates Ca^{2+}-dependent ion channels TMEM16A and SK4 possibly by acting as a counterion channel. *Pflugers Arch.* **459**, 485-497.

Berridge, M. J., Lipp, P. and Bootman, M. D. (2000). The versatility and universality of calcium signalling. *Nat. Rev. Mol. Cell Biol.* **1**, 11-21.

Boon, C. J., Klevering, B. J., Leroy, B. P., Hoyng, C. B., Keunen, J. E. and den Hollander, A. I. (2009). The spectrum of ocular phenotypes caused by mutations in the BEST1 gene. *Prog. Retin. Eye Res.* **28**, 187-205.

Burgess, R., Millar, I. D., Leroy, B. P., Urquhart, J. E., Fearon, I. M., De Baere, E., Brown, P. D., Robson, A. G., Wright, G. A., Kestelyn, P. et al. (2008). Biallelic mutation of BEST1 causes a distinct retinopathy in humans. *Am. J. Hum. Genet.* **82**, 19-31.

Cheng, S. H., Gregory, R. J., Marshall, J., Paul, S., Souza, D. W., White, G. A., O'Riordan, C. R. and Smith, A. E. (1990). Defective intracellular transport and processing of CFTR is the molecular basis of most cystic fibrosis. *Cell* **63**, 827-834.

Clapham, D. E. (1998). The list of potential volume-sensitive chloride currents continues to swell (and shrink). *J. Gen. Physiol.* **111**, 623-624.

Cross, H. E. and Bard, L. (1974). Electro-oculography in Best's macular dystrophy. *Am. J. Ophthalmol.* **77**, 46-50.

Davidson, A. E., Millar, I. D., Urquhart, J. E., Burgess-Mullan, R., Shweikh, Y., Parry, N., O'Sullivan, J., Maher, G. J., McKibbin, M., Downes, S. M. et al. (2009). Missense mutations in a retinal pigment epithelium protein, bestrophin-1, cause retinitis pigmentosa. *Am. J. Hum. Genet.* **85**, 581-592.

Denzer, K., Kleijmeer, M. J., Heijnen, H. F., Stoorvogel, W. and Geuze, H. J. (2000). Exosome: from internal vesicle of the multivesicular body to intercellular signaling device. *J. Cell Sci.* **113**, 3365-3374.

Dykstra, K. M., Pokusa, J. E., Suhan, J. and Lee, T. H. (2010). Yip1A structures the mammalian endoplasmic reticulum. *Mol. Biol. Cell.* **21**, 1556-1568.

Fischmeister, R. and Hartzell, H. C. (2005). Volume sensitivity of the bestrophin family of chloride channels. *J. Physiol.* **562**, 477-491.

Galietta, L. J., Haggie, P. M. and Verkman, A. S. (2001). Green fluorescent protein-based halide indicators with improved chloride and iodide affinities. *FEBS Lett.* **499**, 220-224.

Gouras, P., Braun, K., Ivert, L., Neuringer, M. and Mattison, J. A. (2009). Bestrophin detected in the basal membrane of the retinal epithelium and drusen of monkeys with drusenoid maculopathy. *Graefes Arch. Clin. Exp. Ophthalmol.* **247**, 1051-1056.

Guerois, R., Nielsen, J. E. and Serrano, L. (2002). Predicting changes in the stability of proteins and protein complexes: a study of more than 1000 mutations. *J. Mol. Biol.* **320**, 369-387.

Guziewicz, K. E., Zangerl, B., Lindauer, S. J., Mullins, R. F., Sandmeyer, L. S., Grahn, B. H., Stone, E. M., Acland, G. M. and Aguirre, G. D. (2007). Bestrophin gene mutations cause canine multifocal retinopathy: a novel animal model for best disease. *Invest. Ophthalmol. Vis. Sci.* **48**, 1959-1967.

Hartzell, C., Putzier, I. and Arreola, J. (2005). Calcium-activated chloride channels. *Annu. Rev. Physiol.* **67**, 719-758.

Hartzell, H. C., Qu, Z., Yu, K., Xiao, Q. and Chien, L. T. (2008). Molecular physiology of bestrophins: multifunctional membrane proteins linked to best disease and other retinopathies. *Physiol. Rev.* **88**, 639-672.

Hume, A. N., Buttgereit, J., Al-Awadhi, A. M., Al-Suwaidi, S. S., John, A., Bader, M., Seabra, M. C., Al-Gazali, L. and Ali, B. R. (2009). Defective cellular trafficking of missense NPR-B mutants is the major mechanism underlying acromesomelic dysplasia-type Maroteaux. *Hum. Mol. Genet.* **18**, 267-277.

Jentsch, T. J., Stein, V., Weinreich, F. and Zdebik, A. A. (2002). Molecular structure and physiological function of chloride channels. *Physiol. Rev.* **82**, 503-568.

Kausalya, P. J., Amasheh, S., Gunzel, D., Wurps, H., Muller, D., Fromm, M. and Hunziker, W. (2006). Disease-associated mutations affect intracellular traffic and paracellular Mg^{2+} transport function of Claudin-16. *J. Clin. Invest.* **116**, 878-891.

Kopito, R. R. (1999). Biosynthesis and degradation of CFTR. *Physiol. Rev.* **79**, S167-S173.

Kunzelmann, K., Kongsuphol, P., Aldehni, F., Tian, Y., Ousingsawat, J., Warth, R. and Schreiber, R. (2009). Bestrophin and TMEM16-Ca(2+) activated Cl(-) channels with different functions. *Cell Calcium* **46**, 233-241.

Lang, F. and Paulmichl, M. (1995). Properties and regulation of ion channels in MDCK cells. *Kidney Int.* **48**, 1200-1205.

Liu, L., Done, S. C., Khoshnoodi, J., Bertorello, A., Wartiovaara, J., Berggren, P. O. and Tryggvason, K. (2001). Defective nephrin trafficking caused by missense mutations in the NPHS1 gene: insight into the mechanisms of congenital nephrotic syndrome. *Hum. Mol. Genet.* **10**, 2637-2644.

Marmorstein, A. D., Marmorstein, L. Y., Rayborn, M., Wang, X., Hollyfield, J. G. and Petrukhin, K. (2000). Bestrophin, the product of the Best vitelliform macular dystrophy gene (VMD2), localizes to the basolateral plasma membrane of the retinal pigment epithelium. *Proc. Natl. Acad. Sci. USA* **97**, 12758-12763.

Marmorstein, A. D., Cross, H. E. and Peachey, N. S. (2009). Functional roles of bestrophins in ocular epithelia. *Prog. Retin. Eye Res.* **28**, 206-226.

Milenkovic, V. M., Rivera, A., Horling, F. and Weber, B. H. (2007). Insertion and topology of normal and mutant bestrophin-1 in the endoplasmic reticulum membrane. *J. Biol. Chem.* **282**, 1313-1321.

Milenkovic, V. M., Soria, R. B., Aldehni, F., Schreiber, R. and Kunzelmann, K. (2009). Functional assembly and purinergic activation of bestrophins. *Pflugers Arch.* **458**, 431-441.

Mullins, R. F., Oh, K. T., Heffron, E., Hageman, G. S. and Stone, E. M. (2005). Late development of vitelliform lesions and flecks in a patient with best disease: clinicopathologic correlation. *Arch. Ophthalmol.* **123**, 1588-1594.

Mullins, R. F., Kuehn, M. H., Faidley, E. A., Syed, N. A. and Stone, E. M. (2007). Differential macular and peripheral expression of bestrophin in human eyes and its implication for best disease. *Invest. Ophthalmol. Vis. Sci.* **48**, 3372-3380.

Neussert, R., Muller, C., Milenkovic, V. M. and Strauss, O. (2010). The presence of bestrophin-1 modulates the Ca^{2+} recruitment from Ca^{2+} stores in the ER. *Pflugers Arch.* **460**, 163-175.

O'Driscoll, K. E., Leblanc, N., Hatton, W. J. and Britton, F. C. (2009). Functional properties of murine bestrophin 1 channel. *Biochem. Biophys. Res. Commun.* **384**, 476-481.

Paulson, H. L., Ross, A. F., Green, W. N. and Claudio, T. (1991). Analysis of early events in acetylcholine receptor assembly. *J. Cell Biol.* **113**, 1371-1384.

Petersen, O. H., Tepikin, A. and Park, M. K. (2001). The endoplasmic reticulum: one continuous or several separate Ca(2+) stores? *Trends Neurosci.* **24**, 271-276.

Pianta, M. J., Aleman, T. S., Cideciyan, A. V., Sunness, J. S., Li, Y., Campochiaro, B. A., Campochiaro, P. A., Zack, D. J., Stone, E. M. and Jacobson, S. G. (2003). In vivo micropathology of Best macular dystrophy with optical coherence tomography. *Exp. Eye Res.* **76**, 203-211.

Ponjavic, V., Eksandh, L., Andreasson, S., Sjostrom, K., Bakall, B., Ingvast, S., Wadelius, C. and Ehinger, B. (1999). Clinical expression of Best's vitelliform macular dystrophy in Swedish families with mutations in the bestrophin gene. *Ophthalmic Genet.* **20**, 251-257.

Pusch, M. (2004). Ca(2+)-activated chloride channels go molecular. *J. Gen. Physiol.* **123**, 323-325.

Qu, Z. and Hartzell, H. C. (2008). Bestrophin Cl- channels are highly permeable to HCO3. *Am. J. Physiol. Cell Physiol.* **294**, C1371-C1377.

Qu, Z., Fischmeister, R. and Hartzell, C. (2004). Mouse bestrophin-2 is a bona fide Cl(-) channel: identification of a residue important in anion binding and conduction. *J. Gen. Physiol.* **123**, 327-340.

Qu, Z., Cheng, W., Cui, Y., Cui, Y. and Zheng, J. (2009). Human disease-causing mutations disrupt an N-C-terminal interaction and channel function of bestrophin 1. *J. Biol. Chem.* **284**, 16473-16481.

Rajan, R. S., Illing, M. E., Bence, N. F. and Kopito, R. R. (2001). Specificity in intracellular protein aggregation and inclusion body formation. *Proc. Natl. Acad. Sci. USA* **98**, 13060-13065.

Renner, A. B., Tillack, H., Kraus, H., Kramer, F., Mohr, N., Weber, B. H., Foerster, M. H. and Kellner, U. (2005). Late onset is common in best macular dystrophy associated with VMD2 gene mutations. *Ophthalmology* **112**, 586-592.

Rodriguez-Boulan, E., Kreitzer, G. and Musch, A. (2005). Organization of vesicular trafficking in epithelia. *Nat. Rev. Mol. Cell Biol.* **6**, 233-247.

Rosenthal, R., Bakall, B., Kinnick, T., Peachey, N., Wimmers, S., Wadelius, C., Marmorstein, A. and Strauss, O. (2006). Expression of bestrophin-1, the product of the VMD2 gene, modulates voltage-dependent Ca^{2+} channels in retinal pigment epithelial cells. *FASEB J.* **20**, 178-180.

Rothstein, A. and Mack, E. (1990). Volume-activated K^+ and Cl^- pathways of dissociated epithelial cells (MDCK): role of Ca^{2+}. *Am. J. Physiol.* **258**, C827-C834.

Sanders, C. R. and Myers, J. K. (2004). Disease-related misassembly of membrane proteins. *Annu. Rev. Biophys. Biomol. Struct.* **33**, 25-51.

Shaheen, B., Dang, H. and Fares, H. (2009). Derlin-dependent accumulation of integral membrane proteins at cell surfaces. *J. Cell. Sci.* **122**, 2228-2239.

Shen, M. R., Yang, T. P. and Tang, M. J. (2002). A novel function of BCL-2 overexpression in regulatory volume decrease. Enhancing swelling-activated Ca(2+) entry and Cl(-) channel activity. *J. Biol. Chem.* **277**, 15592-15599.

Stohr, H., Marquardt, A., Nanda, I., Schmid, M. and Weber, B. H. (2002). Three novel human VMD2-like genes are members of the evolutionary highly conserved RFP-TM family. *Eur. J. Hum. Genet.* **10**, 281-284.

Strauss, O. (2005). The retinal pigment epithelium in visual function. *Physiol. Rev.* **85**, 845-881.

Strauss, O., Wiederholt, M. and Wienrich, M. (1996). Activation of Cl- currents in cultured rat retinal pigment epithelial cells by intracellular applications of inositol-1,4,5-triphosphate: differences between rats with retinal dystrophy (RCS) and normal rats. *J. Membr. Biol.* **151**, 189-200.

Sun, H., Tsunenari, T., Yau, K. W. and Nathans, J. (2002). The vitelliform macular dystrophy protein defines a new family of chloride channels. *Proc. Natl. Acad. Sci. USA* **99**, 4008-4013.

Valentijn, J. A., Fyfe, G. K. and Canessa, C. M. (1998). Biosynthesis and processing of epithelial sodium channels in Xenopus oocytes. *J. Biol. Chem.* **273**, 30344-30351.

Varghese, A., Tenbroek, E. M., Coles, J., Jr and Sigg, D. C. (2006). Endogenous channels in HEK cells and potential roles in HCN ionic current measurements. *Prog. Biophys. Mol. Biol.* **90**, 26-37.

von Heijne, G. (1996). Principles of membrane protein assembly and structure. *Prog. Biophys. Mol. Biol.* **66**, 113-139.

Wabbels, B. K., Demmler, A., Preising, M. and Lorenz, B. (2004). Fundus autofluorescence in patients with genetically determined Best vitelliform macular dystrophy: evaluation of genotype-phenotype correlation and longitudinal course. *Invest. Ophthalmol. Vis. Sci.* **45**, e-abstract 1762.

Weingeist, T. A., Kobrin, J. L. and Watzke, R. C. (1982). Histopathology of Best's macular dystrophy. *Arch. Ophthalmol.* **100**, 1108-1114.

Weleber, R. G. (1989). Fast and slow oscillations of the electro-oculogram in Best's macular dystrophy and retinitis pigmentosa. *Arch. Ophthalmol.* **107**, 530-537.

White, K., Marquardt, A. and Weber, B. H. (2000). VMD2 mutations in vitelliform macular dystrophy (Best disease) and other maculopathies. *Hum. Mutat.* **15**, 301-308.

Xiao, Q., Hartzell, H. C. and Yu, K. (2010). Bestrophins and retinopathies. *Pflugers Arch.* **460**, 559-569.

Yu, K., Cui, Y. and Hartzell, H. C. (2006). The bestrophin mutation A243V, linked to adult-onset vitelliform macular dystrophy, impairs its chloride channel function. *Invest. Ophthalmol. Vis. Sci.* **47**, 4956-4961.

Yu, K., Xiao, Q., Cui, G., Lee, A. and Hartzell, H. C. (2008). The best disease-linked Cl- channel hBest1 regulates Ca V 1 (L-type) Ca^{2+} channels via src-homology-binding domains. *J. Neurosci.* **28**, 5660-5670.

Zhang, Y., Stanton, J. B., Wu, J., Yu, K., Hartzell, H. C., Peachey, N. S., Marmorstein, L. Y. and Marmorstein, A. D. (2010). Suppression of Ca^{2+} signaling in a mouse model of Best disease. *Hum. Mol. Genet.* **19**, 1108-1118.

Zhou, Z., Gong, Q., Epstein, M. L. and January, C. T. (1998). HERG channel dysfunction in human long QT syndrome. Intracellular transport and functional defects. *J. Biol. Chem.* **273**, 21061-21066.